Article

Reaction environment impacts charge transfer but not chemical reaction steps in hydrogen evolution catalysis

In the format provided by the authors and unedited

Supplementary Methods

Materials. Palladium foil (99.9%, 0.025 mm thickness) was purchased from Alfa Aesar and pre-treated according to the procedure below. Nickel chloride hexahydrate (99.95%) was obtained from Alpha Aesar and used as received. Palladium (II) sulfate dihydrate (98%) was obtained from Strem Chemicals and used as received. Hydrochloric acid (37 wt.%, 99.999% trace metal basis), sulfuric acid (95.5–96.5%, OmniTrace), lithium hydroxide (99.99%, semiconductor grade) and sodium hydroxide (99.99%, semiconductor grade), sodium perchlorate (99.95%) sodium phosphate dibasic dihydrate (> 99%), sodium phosphate monobasic monohydrate (> 99.5%) and Nafion 117 were obtained from Millipore Sigma and were used as received. Selemion (AMVN, AGC Inc.) was obtained from and soaked in 1 M NaOH for up to 24 h prior to use. Argon (UHP) and hydrogen gas (UHP) were obtained from Airgas and used as received. MilliQ water (Millipore Type 1, 18.2 MΩ cm) was used to make all electrolytes.

General Electrochemical Methods. Biologic VMP 16-channel potentiostats were used for all electrochemical experiments. Ag/AgCl reference electrodes were obtained from BASi Inc. (3 M NaCl) and eDAQ (leakless, ET069). Pt/C (0.5 mg cm^{-2}) gas diffusion electrodes (GDE) were obtained from Fuel Cell Store. Alicat mass flow controllers were used to control gas flow rates to each electrochemical compartment. In all experiments, each solution was sparged with Ar at 10 sccm for at least 30 minutes before any polarization to remove dissolved oxygen from the electrolyte. Electrochemical studies were carried out using custom built gas-tight, glass H-cell parts. All experiments involved the use of two different three-electrode setups, with one comprising the H-pumping cell and the other comprising the analytical cell. The Pd foil membrane acted as the working electrode for both three-electrode setups. The geometric area of the Pd foil was controlled by the o-ring gasket of H-cell joint and was 1 cm^2. All current densities are normalized to this geometric footprint rather than electrochemically active surface area. A Pt mesh or Pd foil was used as counter electrodes (both of which returned identical results).

Three electrochemical cell configurations were used (**Supplementary Fig. 9**). The first configuration (**Supplementary Fig. 9a**) contained two separated three electrode cells (the H-pumping and analytical cells) with a common Pd membrane working electrode. For each three electrode cell, the working (Pd) and counter (Pd or Pt) electrodes were not separated by a membrane separator. The second configuration (**Supplementary Fig. 9b**) contained a Nafion membrane separating working and counter compartments of the H-pumping cell; working and counter electrodes remained unseparated in the analytical cell. The third configuration (**Supplementary Fig. 9c**) contained membrane separators between working and counter compartments in both the H-pumping and analytical cells. Nafion was employed as the separator when the electrolyte was acidic and neutral, and Selemion was employed for alkaline electrolytes. It was found that the inclusion of a membrane separator had no appreciable effect on the electrochemical response of the system, and, as such, most of the data were collected using no membrane separators in either the H-pumping or analytical cells (configuration in **Supplementary**

Fig. 9a). All cell components were cleaned prior to use by immersion in concentrated sulfuric acid for at least 1 h, followed by copious rinsing with Milli-Q water and drying under flowing Ar.

During all experiments, the electrochemical double cell was placed on a VWR 200 Rocking Platform Shaker set to rock at setting 2 to dislodge H_2 bubbles generated at the Pd interface during electrolysis.

In-Line Gas Quantitation. H_2 gas emanating from the analytical compartment was quantified by in-line gas chromatography using an SRI Instruments, Multi-Gas Analyzer, Model 8610C equipped with a thermal conductivity detector and a 2 m ShinCarbon (Restek) column. For experiments containing CO, in-line H_2 quantitation was conducted using an in-line gas chromatograph (SRI Instruments, Multi-Gas Analyzer, Model 8610C) equipped with a thermal conductivity detector and two MolSieve 13X and Hayesep D columns connect in series.

Palladium Preparation. Pd foil electrodes were cleaned and palladized prior to use in the electrochemical double cell. For the cleaning step, the Pd membrane double cell was assembled, with a 1 cm^{-2} geometric surface area of Pd exposed to the electrolyte in the analytical and H-pumping cells. Both sides of the Pd foil were first simultaneously cleaned by CV cycling in 1 M H_2SO_4 electrolyte under a continuous 10 sccm Ar sparge. CV cycling commenced at the open circuit potential (OCP) scanning negative at 50 mV s^{-1} scan rate. The electrode was cycled between 0.1 and 1.1 V vs. Ag/AgCl (3 M NaCl) for 100 cycles. This cleaning procedure was conducted using a Pt mesh or Pd foil counter electrode. Both sides of the foil were then thoroughly washed with Milli-Q water (without disassembling the double cell).

Following cleaning by CV cycling, the Pd foil was retained in the same electrochemical double cell, and both sides of the Pd working electrode were palladized. A fresh 15.9 mM $PdSO_4$ solution in 1 M HCl was used for each palladization preparation. A Ag/AgCl (3 M NaCl) electrode and a Pt mesh or Pd foil were used as the reference and counter electrodes respectively on each compartment. The H-pumping and analytical cell compartments were each filled with 10 mL of the palladization solution, and each face of the Pd working electrode was simultaneously polarized potentiostatically to −0.2 V versus Ag/AgCl (3 M NaCl) without iR compensation until 7.38 C cm^{-2} of charged. The palladization procedure was carried out under a continuous 10 sccm Ar sparge. The palladized Pd foil was then thoroughly washed with Milli-Q water (without disassembling the double cell) and dried in flowing Ar.

Electrochemical deposition of Ni(OH)₂ onto Pd. The analytical compartment was charged with 10 mL of 0.005 M $Ni(Cl)_2 \cdot 6H_2O$ electrolyte. The palladized Pd foil was then Galvanostatically polarized at +400 μA for 15 minutes in a two-electrode setup with a Pt mesh as the counter electrode. The foil was then thoroughly washed with Milli-Q water (without disassembling the double cell) and dried in flowing Ar.

Determining the chemical overpotential-rate scaling for H$_2$ release. Measurements of the OCP at the analytical interface at varying currents passed at the H-pumping interface were performed with the following setup: For the H-pumping cell, a Ag/AgCl (3 M NaCl) was used as the reference electrode and a Pt mesh or Pd foil was used as the counter electrode. In all experiments, the electrolyte used in the H-pumping cell was 1 M H$_2$SO$_4$. The H-pumping cell was also sparged with 10 sccm Ar, although replacing the gas with H$_2$ did not affect any of the measurements. For the analytical cell, a hanging strip Pt GDE was used as the reference electrode (which operates as a RHE when under an H$_2$ atmosphere) and either a Pt mesh or Pd foil was used as the counter electrode. The analytical cell was sparged with 10 sccm H$_2$, although no difference in potential between the additional reference and the Pd working electrode was observed when H$_2$ was replaced with Ar (however, the Pt GDE would no longer be capable of acting as a reference electrode). Electrolytes used in the analytical cell included 1 M H$_2$SO$_4$ (pH = 0.6), 1 M sodium hydroxide (pH =13.6), 1 M lithium hydroxide (pH =13.6), 0.5 M sodium formate + 0.5 M sodium borate + 1 M sodium perchlorate buffer (pH = 7.3), 0.5 M sodium acetate + 0.5 M sodium borate + 1 M sodium perchlorate buffer (pH = 7.3) and 1 M sodium phosphate + 1 M sodium perchlorate buffer (pH = 6.3) (**Fig. 3**). All experiments involving Ni(OH)$_2$ were conducted in 1 M sodium hydroxide (pH = 13.6) (**Supplementary Fig. 6a**).

For measurement of the OCP of the analytical interface, the H-pumping interface was galvanostatically polarized at current densities ranging from −1 to −100 mA cm^{-2}. During each galvanostatic electrolysis, the OCP was recorded in the analytical cell. Galvanostatic polarization on the H-pumping cell was held until the OCP at the analytical interface reached as stable value, which took anywhere from 1 to 20 minutes. These steady-state open circuit values at the analytical interface provided the Y-axis data points in **Fig. 3a, Fig. 3d**, **Supplementary Fig. 5a** and **Supplementary Fig. 6a**.

For measurements of the H$_2$ permeation rate at the analytical interface under Galvanostatic polarization at the H-pumping interface, the following set up was employed: For the H-pumping cell, a Ag/AgCl (3 M NaCl) was used as the reference electrode and a Pt mesh or Pd foil was used as the counter electrode. A three-compartment cell was used such that the working and counter electrodes of the H-pumping cell were separated by a Nafion membrane. The electrolyte used was 1 M H$_2$SO$_4$ in all experiments. For the analytical cell, a Ag/AgCl (3 M NaCl in acid and neutral electrolytes, leakless in alkaline electrolytes) was used as the reference electrode and either a Pt mesh or Pd foil was used as the counter electrode. Both cells were sparged independently with Ar at 10 sccm. The current density at the H-pumping interface ranged from −10 to −100 mA cm^{-2}, and the analytical interface was held at the OCP for the duration of the experiment. The outflow of the analytical compartment was analyzed via GC to measure the amount of H$_2$ that permeated across the Pd membrane. In each experiment, galvanostatic electrolysis at the H-pumping interface was maintained for 30 minutes, which afforded enough time to reach a steady state H$_2$ evolution rate at analytical interface as judged by a stable GC response. The recorded OCP values at the analytical interface was converted to the reversible hydrogen electrode (RHE) scale using the following equation, (E$_{RHE}$ = E$_{Ag/AgCl}$ + 0.210 V + 0.059V×pH), and were unchanged from the

4

potentials measured under a H_2 atmosphere using the RHE reference electrode in the experiments mentioned above.

H_2 evolution in analytical cell compartment was measured using an in-line gas chromatograph and detected using the equipped thermal conductivity detector. A 2 m ShinCarbon (Restek) column with an isothermal temperature program (165 °C) and Ar carrier gas (UHP, Airgas, 20 psi) were used to separate H_2 from possible contaminant gasses (O_2 or N_2), which were not observed in the effluent from either cell. GC traces were collected every 3 min from a 0.5 mL sample loop injection. The concentration of H_2 was determined via integrated peak area via a calibration curve. The partial current density for H_2 was calculated using the following equation:

$$j_i = c_i * n_i * F * V_{gas} * \frac{P}{RT} * \frac{1}{A}$$ (1)

where c_i is the GC detected product in ppm, n_i is the electron stoichiometry for the H_2 product, 2, F is Faraday's constant (96485 C mol^{-1}), V_{gas} is the substrate gas flow rate (10 sccm in all cases), P is the pressure in the cell (1 atm), A is the sample surface area, R is the gas constant and T is temperatures.

To establish a chemical overpotential-rate scaling for H_2 release, the deviation of the OCP from RHE at the analytical interface (measured from OCP experiments under both a H_2 and Ar atmosphere) was plotted against the log rate of H_2 release measured at that same interface. Chemical overpotential-rate scaling for H_2 release relationships were obtained for electrolytes in the analytical cell including 1 M H_2SO_4 acid (pH = 0.6), 1 M sodium hydroxide (pH = 13.6), and 1 M sodium phosphate + 1 M sodium perchlorate buffer (pH = 6.3). The foregoing procedure generated the data in **Fig. 4**. All experiments involving Ni(OH)$_2$ were conducted in 1 M NaOH and generated the data in **Fig. 5b**.

Determining the chemical overpotential-rate scaling for H_2 release in the presence of CO. For studies that examined the effect of CO poisoning on the Pd membrane double cell, slight modifications to the above method were applied: The electrolyte used in both the H-pumping and analytical cell was 1 M H_2SO_4. For the H-pumping cell, a Ag/AgCl (3 M NaCl) was used as the reference electrode and a Pt mesh or Pd foil was used as the counter electrode. The H-pumping cell was sparged with 10 sccm Ar for the duration of the experiment. For the analytical cell, a Ag/AgCl (3 M NaCl) was used as the reference electrode and either a Pt mesh or Pd foil was used as the counter electrode. The analytical cell was initially sparged with 10 sccm Ar, and switched to 20 sccm CO during the course of the experiment. To measure the chemical overpotential, galvanostatic polarization with current densities ranging from −1 to −100 mA cm^{-2} was performed at the H-pumping cell, and the OCP was measured on the analytical cell (**Supplementary Fig. 5a**). Galvanostatic polarizations on the H-pumping cell was held until the open circuit response stabilized, which took anywhere from 1 to 20 minutes. The recorded OCP values at the analytical

interface was converted to the reversible hydrogen electrode (RHE) scale using the following equation, ($E_{RHE} = E_{Ag/AgCl} + 0.210$ V + 0.059V×pH).

The same cell setup was used to measure H_2 permeation rates at the analytical interface under CO poisoning conditions. H_2 was measured using an in-line gas chromatograph and detected using the equipped thermal conductivity detector. Both cells were initially sparged independently with Ar at 10 sccm. Then, the sparge gas in the analytical cell was switched to CO at 20 sccm. The current density at the H-pumping interface ranged from −10 to −100 mA cm^{-2}, and the analytical interface was held at OCP for the duration of the experiment. The outflow of the analytical compartment was analyzed via gas chromatography to measure the amount of H_2 permeation across the Pd membrane (**Supplementary Fig. 5b**). All gaseous products were identified and quantified following a GC analysis methodology described in the literature.[1] The partial current density for H_2 was calculated using the same above equation. Each H-pumping current was maintained for 40 minutes, which yielded a stable GC response for H_2 detection.

To establish a chemical overpotential-rate scaling for H_2 release with CO poisoning, the deviation of the OCP from RHE at the analytical interface was plotted against the log rate of H_2 release measured at that same interface to produce the plot in **Fig. 5a**.

Isolating the charge transfer overpotential component for passing current at the analytical interface (with and without CO).

For experiments isolating the charge transfer overpotential component for H_2 catalysis (**Fig. 6** and **Fig. 7**), simultaneous polarization of both the H-pumping and analytical interfaces of the Pd membrane was performed. In all experiments, the current density at the H-pumping interface was maintained at −100 mA cm^{-2}. Simultaneously, current was passed at the analytical interface. For experiments that did not involve CO (**Fig. 6** and **Fig. 7b**), the analytical compartment was sparged with H_2 at 10 sccm, and Pt GDE was used as the reference electrode. Current densities at the analytical interface ranged from −30 to 30 mA cm^{-2}, with galvanostatic polarization held until the potential at the analytical interface reached steady state (between 5–10 minutes). For unmodified Pd electrodes, the electrolytes used in the analytical cell included 1 M H_2SO_4 acid (pH = 0.6), 1 M sodium hydroxide (pH = 13.6) and 1 M sodium phosphate + 1 M sodium perchlorate buffer (pH = 6.3) and produced the data in **Fig. 6**. All experiments involving $Ni(OH)_2$ modified Pd were conducted in 1 M sodium hydroxide (pH = 13.6) and produced the data in **Fig. 7b**. For experiments that involved CO, the analytical compartment was sparged with CO at 20 sccm and a Ag/AgCl (3 M NaCl) was used as a reference electrode. Current densities at the analytical interface ranged from −3 to 0 mA cm^{-2}. Oxidative currents could not be sampled under CO as measured potentials were unstable and did not reach steady state. This procedure generated the data in **Fig. 7a**.

Fitting of double polarization Butler-Volmer plots was performed in MATLAB (version 2021b) via a non-linear least squares method. The experimental current density (j) and potential (E) data were fit to the logarithm of the absolute value of the Butler-Volmer equation:

$$\log_{10}|j| = \log_{10}\left|j_0 e^{\alpha\frac{F(E-E_0)}{RT}} - j_0 e^{-(1-\alpha)\frac{F(E-E_0)}{RT}}\right| \tag{2}$$

where F is Faraday's constant, R is the ideal gas constant, and T is the temperature (300 K). The equilibrium potential (E_0) exchange current density (j_0), and the symmetry factor (α) were parameters determined from the fitting procedure. When the current density is large or more polarized, it is convoluted by a non-negligible shift in chemical overpotential at steady state. To minimize the effect of this convolution on the fit, the data points were weighted by the reciprocal of the absolute value of j. The average of the least polarized anodic and cathodic potentials was used as the starting value the equilibrium potential. A symmetry factor of 0.5 and current density of 1.0 nA cm^{-2} were used for the other starting values. Data fitting was used to produce the plot in **Supplementary Fig. 7**.

Supplementary Discussion

1. Definition of the Chemical Overpotential:

We first define the chemical potential of H under non-equilibrium steady state catalysis in terms of the activity of H:

$$\mu_H = RT \ln a_H \qquad \textbf{Eq. 1}$$

We define the standard state chemical potential, $\mu_{H,0}$, as the chemical potential of surface H in equilibrium with 1 atm of H_2:

$$\mu_{H,0} = RT \ln a_{H,0} \qquad \textbf{Eq. 2}$$

Combining **Eq. 1** and **Eq. 2**:

$$\mu_H - \mu_{H,0} = RT \ln \frac{a_H}{a_{H,0}} \qquad \textbf{Eq. 3}$$

This difference in chemical potential can be converted to voltage units by dividing by Faraday's constant, F, to arrive at the definition of chemical overpotential, $\eta_{chemical}$ as given in **Eq. 1** in the main text:

$$\eta_{chemical} = \frac{\mu_H - \mu_{H,0}}{F} = \frac{RT}{F} \ln \frac{a_H}{a_{H,0}} \qquad \textbf{Eq. 4}$$

2. Relating the Open Circuit Potential at the Analytical Interface to the Chemical Overpotential for HER.

In a Volmer-Tafel mechanism, there are two steps, each of which have their own distinct electrochemical free energies $\Delta \bar{G}$. For the Volmer reaction, $\Delta \bar{G}_V$ can be expressed with the following relationship:

$$\Delta \bar{G}_V = \Delta G_V + FE = \Delta G_V^0 + FE - RT\ln\left(\frac{a_{H^+}}{a_H}\right) \qquad \textbf{Eq. 5}$$

At standard state activity for H$^+$ and surface H, the last term cancels, giving:

$$\Delta \bar{G}_V = \Delta G_V^0 + FE \qquad \textbf{Eq. 6}$$

At equilibrium, $\Delta \bar{G}_V = 0$, and $E = E_{H^+/H_{OPD}}^0$, thus,

$$\Delta G_V^0 = -FE_{H^+/H_{OPD}}^0 \qquad \textbf{Eq. 7}$$

Similarly, for the Tafel reaction, $\Delta \bar{G}_T$ can be expressed with the following relationship:

$$\Delta \bar{G}_T = \Delta G_T = \Delta G_T^0 - RT\ln\left(\frac{a_H}{a_{H_2}^{0.5}}\right) \qquad \textbf{Eq. 8}$$

At equilibrium (i.e. $\Delta \bar{G}_T = 0$), the activities of H$_2$ and surface H are equilibrated such that

$$0 = \Delta G_T^0 - RT\ln\left(\frac{a_{H,eq}}{\left(a_{H_2}^{0.5}\right)_{eq}}\right) \qquad \textbf{Eq. 9}$$

Rearranging **Eq. 9** provides an expression for ΔG_T^0:

$$\Delta G_T^0 = RT\ln\left(\frac{a_{H,eq}}{\left(a_{H_2}^{0.5}\right)_{eq}}\right) \qquad \textbf{Eq. 10}$$

Substituting **Eq. 10** into **Eq. 8** yields the following relationship:

$$\Delta \bar{G}_T = RT\ln\left(\frac{a_{H,eq}}{\left(a_{H_2}^{0.5}\right)_{eq}}\right) - RT\ln\left(\frac{a_H}{a_{H_2}^{0.5}}\right)$$

$$-\Delta \bar{G}_T = RT\ln\left(\frac{a_H}{a_{H,eq}} \times \frac{\left(a_{H_2}^{0.5}\right)_{eq}}{a_{H_2}^{0.5}}\right) \qquad \textbf{Eq. 11}$$

Assuming that $a_{H_2}^{0.5} = \left(a_{H_2}^{0.5}\right)_{eq}$ (i.e. in the limit that the H_2 activity is unchanged in its out of equilibrium state), **Eq. 11** can be simplified to the following equation:

$$-\Delta \bar{G}_T = RT\ln\left(\frac{a_H}{a_{H,eq}}\right)$$

Eq. 12

Notably, $a_{H,eq} = a_{H,0}$ when referencing to the equilibrium activity of surface H under 1 atm H_2 (under standard state conditions). Thus, the change in free energy for the Tafel step relative to the standard state conditions (1 atm H_2), in the limit of unchanged H_2 activity can be expressed as:

$$-\Delta \bar{G}_T = RT\ln\left(\frac{a_H}{a_{H,0}}\right)$$

Eq. 13

Eq. 13 with **Eq. 4** are related by the following expression:

$$\frac{-\Delta \bar{G}_T}{F} = \frac{RT}{F}\ln\frac{a_H}{a_{H,0}} = \eta_{chemical}$$

Eq. 14

The standard state potential for the overall HER can be obtained from the sum of the Volmer and Tafel free energy changes at standard state such that:

$$\Delta G_V^0 + \Delta G_T^0 = -FE_{H^+/H_2}^0$$

Eq. 15

The measured OCP at the analytical interface is assumed to be set by the quasi-equilibrated Volmer reaction but at a non-equilibrium H activity relative to H_2. Thus, the OCP reports on the deviation of the Volmer reaction from its standard state:

$$E_{OCP} = E_V = E_{H^+/H_{OPD}}^0 + \frac{RT}{F}\ln\left(\frac{a_{H^+}}{a_H}\right)$$

Eq. 16

Substituting in $\Delta G_V^0 = -FE_{H^+/H_{OPD}}^0$:

$$E_{OCP} = -\frac{\Delta G_V^0}{F} + \frac{RT}{F}\ln\left(\frac{a_{H^+}}{a_H}\right)$$

Eq. 17

Substituting in $\frac{\Delta G_V^0}{F} = -\frac{\Delta G_T^0}{F} - E_{H^+/H_2}^0$ (from **Eq. 15**):

$$E_{OCP} = -\left(-\frac{\Delta G_T^0}{F} - E_{H^+/H_2}^0\right) + \frac{RT}{F}\ln\left(\frac{a_{H^+}}{a_H}\right)$$

Eq. 18

This can be rearranged as:

$$E_{OCP} = -\left(-\frac{\Delta G_T^0}{F} + \frac{RT}{F}\ln(a_H)\right) + E_{H^+/H_2}^0 + \frac{RT}{F}\ln(a_{H^+}) \qquad \textbf{Eq. 19}$$

Isolating $\left(-\frac{\Delta G_T^0}{F} + \frac{RT}{F}\ln(a_H)\right)$ gives the following expression:

$$-\frac{\Delta G_T^0}{F} + \frac{RT}{F}\ln(a_H) = -\left(E_{OCP} - \left(E_{H^+/H_2}^0 + \frac{RT}{F}\ln(a_{H^+})\right)\right) \qquad \textbf{Eq. 20}$$

Subtracting $\frac{RT}{F}\ln\left(\left(a_{H_2}^{0.5}\right)_0\right)$ on both sides yields:

$$-\frac{\Delta G_T^0}{F} + \frac{RT}{F}\ln\left(\frac{a_H}{\left(a_{H_2}^{0.5}\right)_0}\right) = -\left(E_{OCP} - \left(E_{H^+/H_2}^0 + \frac{RT}{F}\ln\left(\frac{a_{H^+}}{\left(a_{H_2}^{0.5}\right)_0}\right)\right)\right) \qquad \textbf{Eq. 21}$$

In the limit that the activity of H$_2$ at the electrode surface is equal to the equilibrium value considered at RHE potential (i.e. $a_{H_2}^{0.5} = \left(a_{H_2}^{0.5}\right)_{eq} = \left(a_{H_2}^{0.5}\right)_0$) **Eq. 8** can be rearranged and expressed in this system as:

$$\frac{\Delta \bar{G}_T}{F} = \frac{\Delta G_T^0}{F} - \frac{RT}{F}\ln\left(\frac{a_H}{\left(a_{H_2}^{0.5}\right)_0}\right) \qquad \textbf{Eq. 22}$$

Substituting **Eq. 22** into **Eq. 21** yields:

$$-\frac{\Delta \bar{G}_T}{F} = -\left(E_{OCP} - \left(E_{H^+/H_2}^0 + \frac{RT}{F}\ln\left(\frac{a_{H^+}}{\left(a_{H_2}^{0.5}\right)_0}\right)\right)\right) \qquad \textbf{Eq. 22}$$

Note that $\left(FE_{H^+/H_2}^0 + \frac{RT}{F}\ln\left(\frac{a_{H^+}}{\left(a_{H_2}^{0.5}\right)_0}\right)\right)$ is the RHE potential, and thus, $E_{OCP} - \left(E_{H^+/H_2}^0 + \frac{RT}{F}\ln\left(\frac{a_{H^+}}{\left(a_{H_2}^{0.5}\right)_0}\right)\right)$ refers to the potential E_{OCP} against the RHE potential. Therefore:

$$-\frac{\Delta \bar{G}_T}{F} = -E_{OCP} \ (V \ vs. RHE) \qquad \textbf{Eq. 24}$$

Finally, substituting $-\frac{\Delta \bar{G}_T}{F} = \eta_{chemical}$ (**Eq. 12**) yields the following relationship:

$$\eta_{chemical} = -E_{OCP} \ (V \ vs. RHE) \qquad \textbf{Eq. 25}$$

3. Derivation of the Calculated 30 mV dec^{-1} Tafel slope for a Tafel rate limiting mechanism

Consider the Volmer-Tafel Mechanism:

Volmer step: $\qquad$ $H^+ + Pd + e^- \rightleftharpoons Pd\text{-}H_{OPD}$ $\qquad\qquad$ (3)

Heyrovsky step: $\qquad$ $H^+ + Pd\text{-}H_{OPD} + e^- \rightleftharpoons Pd + H_2$ $\qquad\qquad$ (4)
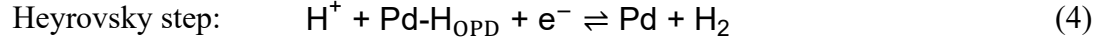
In a Tafel limited HER mechanism, we assume that the Volmer step is in equilibrium such that its potential can be described by the Nernst Equation:

$$E_V = E^0_{H^+/H_{OPD}} - \frac{RT}{F}\ln\left(\frac{a_H}{a_H^+}\right)$$

$$E_V = E^0_{H^+/H_{OPD}} - \frac{RT}{F}\ln(a_H) + \frac{RT}{F}\ln(a_H^+) \qquad\qquad \textbf{Eq. 26}$$

The rate of the HER, can also be described as the forward rate of the Tafel reaction:

$$i \times F = 2v_{Tafel} = k_{Tafel}a_H^2 \qquad\qquad \textbf{Eq. 27}$$

Where i is the current passed and k_{Tafel} is the forward potential independent rate constant for the Tafel reaction. We assume there is no reverse Tafel process as Tafel is rate limiting.

Eq. 27 can be rearranged to isolate a_H:

$$a_H = \left(i \times \frac{F}{k_{Tafel}}\right)^{0.5} \qquad\qquad \textbf{Eq. 28}$$

Substituting **Eq. 28** into **Eq. 26** yields:

$$E_V = E^0_{H^+/H_{OPD}} - \frac{RT}{F}\ln\left(\left(i \times \frac{F}{k_{Tafel}}\right)^{0.5}\right) + \frac{RT}{F}\ln(a_H^+) \qquad\qquad \textbf{Eq. 29}$$

The natural logarithm $\frac{RT}{F}ln(i^{0.5})$ can be approximated as $\frac{0.059}{2}\log(i)$, and thus **Eq. 29** can be rewritten in the following form:

$$E_V = E^0_{H^+/H_{OPD}} - \frac{RT}{F}\ln\left(\left(\frac{F}{k_{Tafel}}\right)^{0.5}\right) + \frac{RT}{F}\ln(a_H^+) - \frac{0.059}{2}\log(i) \qquad\qquad \textbf{Eq. 30}$$

Taking the derivative of E_V with respects to $\log(i)$ yields:

$$\frac{dE_V}{d\log(i)} = -\frac{0.059}{2} \text{ mV dec}^{-1} \qquad\qquad \textbf{Eq. 31}$$

Thus, the Tafel slope, $\left|\frac{dE}{d\log(i)}\right|$, for a Tafel rate limiting mechanism of the HER is $29.5 \approx 30$ mV dec^{-1}

4. Incorporation of net attractive or repulsive interactions via a Frumkin isotherm and the effect on Tafel slopes

In describing the thermodynamics of an adsorbed species, it is often assumed that the species behaves Langmuirian. In this simplified picture of adsorption, neighboring species are non-interacting. A more nuanced description accounts for the possibility of net attractive or repulsive interactions that become relevant as the surface becomes more saturated. In the limit where these interactions exhibit a linear free energy relation with surface coverage the adsorption follows a Frumkin isotherm:[2]

$$\frac{\theta}{1-\theta} e^{-g\theta/RT} = K[H_3O^+]e^{-FE/RT} \qquad \textbf{Eq. 33}$$

where θ is the surface coverage and K is the equilibrium constant of the electrochemical adsorption of a hydrogen atom via the Volmer reaction. The term g is the H-interaction parameter and is the average interaction energy between neighboring adsorbed H-species when the surface is saturated (when θ is 1). All other variables are as defined in the discussion above. Notably, in the case where g is zero, the equation simplifies to the familiar Langmuirian isotherm.

To calculate the effect that net attractive or net repulsive interactions would have on the observed rate scaling for H$_2$ release with chemical overpotential in a Volmer–Tafel mechanism, we calculated the change in potential and change in rate (**Supplementary Fig. 4**). We set several inconsequential constants – the Tafel rate constant, the Volmer equilibrium constant, and the activity of hydronium – as unity. These constants only serve to translate the resulting trend with respect to the logarithm of rate or potential. Consistent with this, we have intentionally depicted the axes without units in **Supplementary Fig. 4**.

The simulated Tafel slopes in **Supplementary Fig. 4** were calculated by finite differences. For a range of thetas from 0 to 1 with a spacing of 0.001, we calculated the logarithm of the Tafel rate ($\log \theta^2$). The potential was solved from the Frumkin isotherm equation (at a set g, using the numerical solving functionality in Matlab version 2022b). The Tafel slope was then obtained by taking the difference between potentials of neighboring theta values divided by the difference in the logarithm of their rate:

$$\frac{\partial E}{\partial \log j} \approx \frac{\Delta E}{\Delta \log j} = \frac{E_{\theta_0} - E_{\theta_0+0.001}}{\log j_{\theta_0} - \log j_{\theta_0+0.001}} \qquad \textbf{Eq. 34}$$

This calculation was done for the integer values of g from -4 to 2.
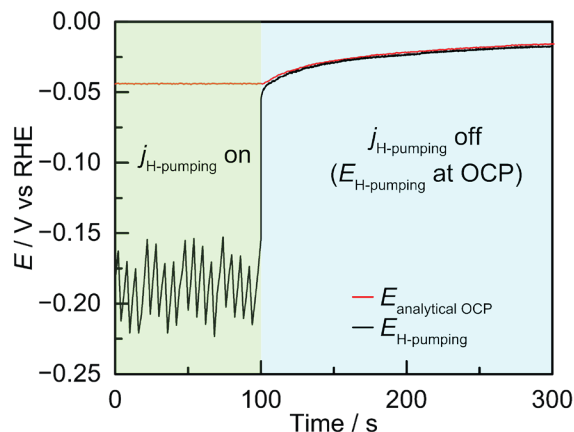
Supplementary Figure 1. Potential of both the H-pumping interface (black) and the analytical interface (red) under galvanostatic polarization of -100 mA cm^{-2} at the H-pumping interface (green region) and immediately after polarization is turned off (blue region).

Upon termination of polarization, the open circuit potential (OCP) on both interfaces collapses to the same value (we observe a consistent offset of approximately 2 mV which we ascribe to a slight offset between reference electrodes). Furthermore, both OCP values decay towards more positive values together. Taken together, we believe that the minimal deviation in OCP between the H-pumping and analytical interface post electrolysis suggests that the chemical potential difference of surface H between the H-pumping and analytical interface is minimal, which would be consistent with a system that is not under diffusion limitations.
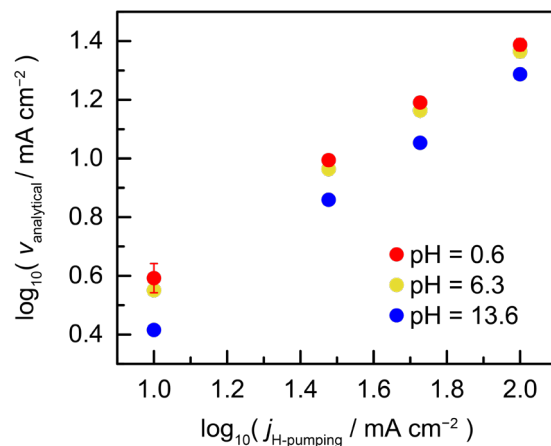
Supplementary Figure 2. Rate of H_2 release at the analytical interface ($v_{analytical}$) versus the total current passed at the H-pumping interface ($j_{H\text{-pumping}}$) under different pH conditions including 13.6 (blue), 6.3 (yellow) and 0.6 (red). Data points are presented as mean values and error bars indicate standard deviations obtained from triplicate ($n = 3$) measurements (some error bars are smaller than the data point markers).
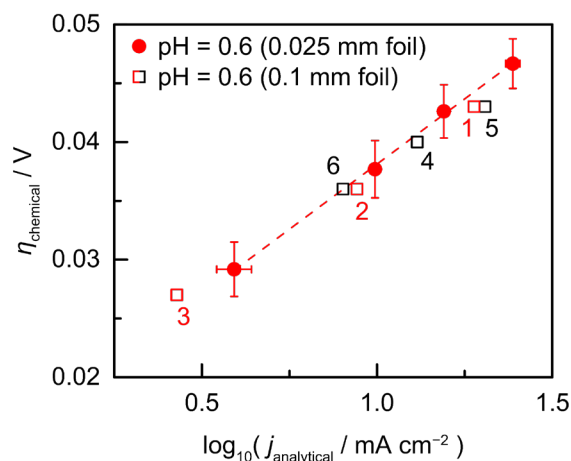
Supplementary Figure 3. The rate of H_2 release at the analytical interface ($v_{analytical}$) versus the chemical overpotential at that interface ($\eta_{chemical}$) for a 0.025 mm (red circles) and 0.1 mm thick Pd foil (red and black open squares). Data points are presented as mean values and error bars indicate standard deviations obtained from triplicate ($n = 3$) measurements (some error bars are smaller than the data point markers). The 0.1 mm thick Pd foil experiment was performed only once via a staircase electrolysis program on the H-pumping interface. The numbers correspond to the sequence in which electrolysis conditions were applied. Potentials were measured with a Ag/AgCl reference electrode calibrated to the RHE.

The use of a thicker Pd foil results in a largely unchanged scaling of H_2 release at the analytical interface with $\eta_{chemical}$ measured, suggesting that the influence of H diffusion through the Pd membrane has nominal effect on the interfacial surface H chemistry occurring at the analytical interface.
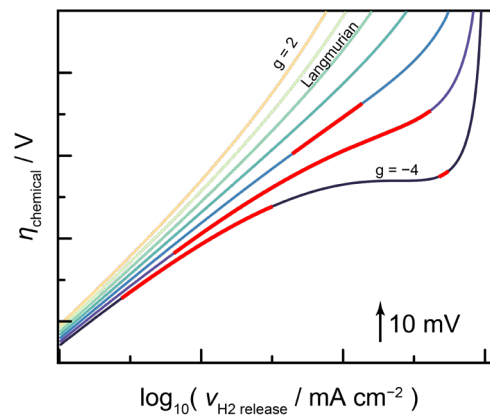
Supplementary Figure 4. The rate of H$_2$ release with chemical overpotential modelled for a Langmuirian isotherm, and also Frumkin isotherms with both repulsive (g > 0) and attractive (g < 0) interactions. The red regions denote where a 20 ± 5 mV dec^{-1} rate scaling for H-H recombination with chemical overpotential would be observed. Details of the modelling are provided in **Supplementary Discussion 4**.

a

$E_{\text{analytical OCP}}$ / V vs RHE

14.2 mV dec^{-1}

17.4 mV dec^{-1}

● Ar
○ CO

$\log_{10}(j_{\text{H-pumping}} / \text{mA cm}^{-2})$

b

$\log_{10}(v_{\text{analytical}} / \text{mA cm}^{-2})$

● Ar
○ CO

$\log_{10}(j_{\text{H-pumping}} / \text{mA cm}^{-2})$

c

Formic Acid
^{1}H NMR (500 MHz, CD$_3$CN)

— Before experiment
— After experiment
- - 0.1 M Formic acid

δ (ppm)
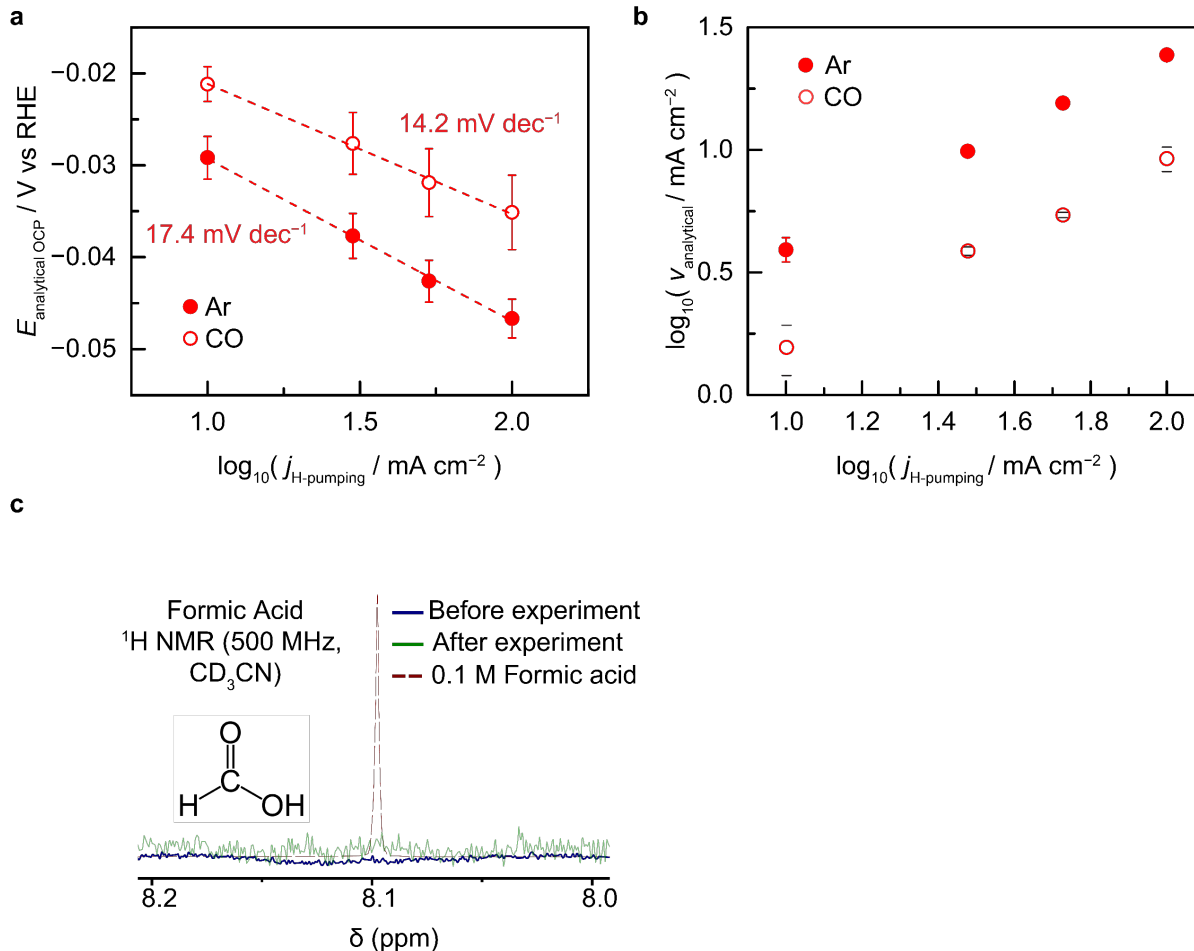
Supplementary Figure 5. CO poisoning effects on the Pd electrochemical double cell. **(a)** Open circuit potential dependence of the analytical interface ($E_{\text{analytical OCP}}$) under Galvanostatic polarization at the H-pumping interface ($j_{\text{H-pumping}}$), with CO (open red circles) and without CO (closed red circles). Data points are presented as mean values and error bars indicate standard deviations obtained from triplicate ($n = 3$) measurements. **(b)** The rate of H$_2$ evolution at the analytical interface ($j_{\text{analytical}}$) versus the current density passed at the H-pumping interface ($j_{\text{H-pumping}}$), with CO (open red circles; data points are presented as mean values of $n = 2$ measurements, with black lines showing the absolute difference between duplicate points) and without CO (closed red circles; data points are presented as mean values, and error bars indicate standard deviation from $n = 3$ measurements; some error bars are smaller than the data point markers). **(c)** ^{1}H NMR spectra of the electrolyte pre- and post-electrolysis (blue and green, respectively), showing no detectable formic acid from electrolysis under CO. ^{1}H NMR reference spectra of 0.1 M formic acid (dotted line).

18
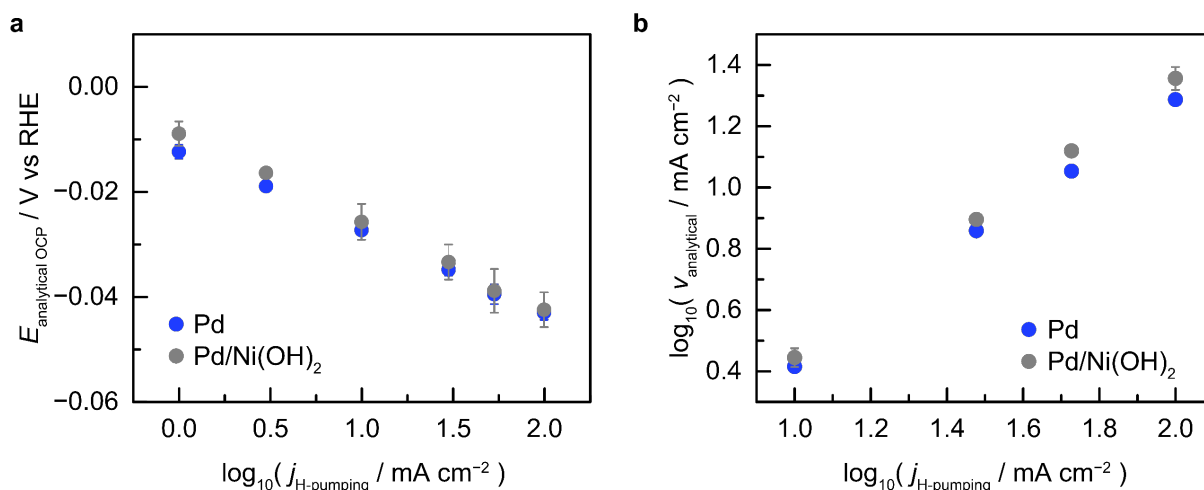
Supplementary Figure 6. **(a)** Open circuit potential dependence of the analytical interface ($E_{\text{analytical OCP}}$) under Galvanostatic polarization at the H-pumping interface ($j_{\text{H-pumping}}$), with (blue) and without Ni(OH)$_2$ (grey) in 1 M NaOH. **(b)** The rate of H$_2$ evolution at the analytical interface ($j_{\text{analytical}}$) versus the current passed at the H-pumping interface ($j_{\text{H-pumping}}$), with (blue) and without Ni(OH)$_2$ (grey) in 1 M NaOH. Data points are presented as mean values and error bars indicate standard deviations obtained from triplicate ($n = 3$) measurements (some error bars are smaller than the data point markers).
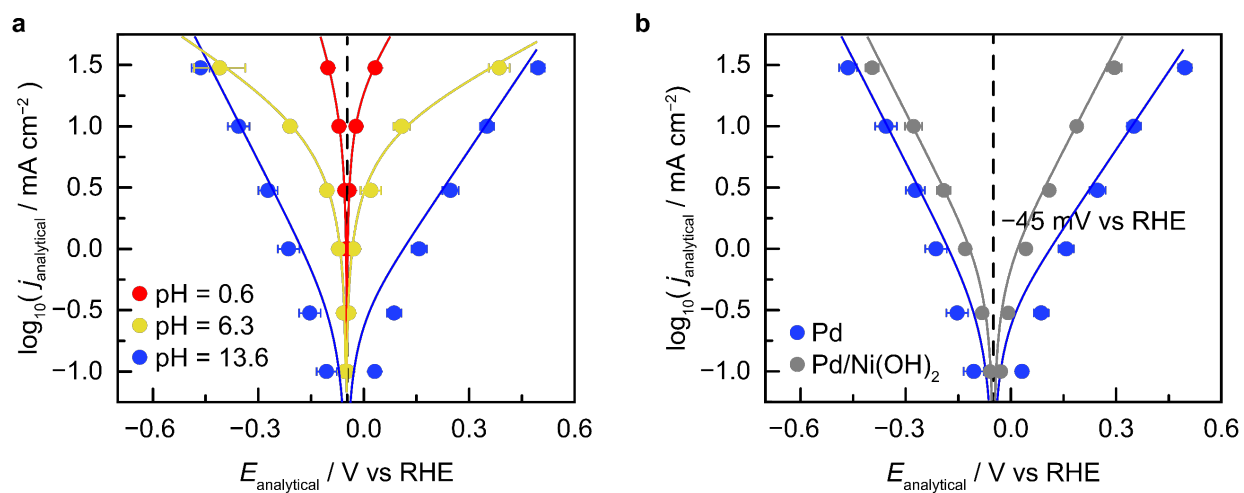
Supplementary Figure 7. Fitting the double polarization Butler-Volmer plots for (**a**) pH = 0.6 (red), pH = 6.3 (yellow) and pH = 13.6 (blue) and (**b**) pH = 13.6 on bare (blue) and Ni(OH)$_2$ decorated Pd (grey). Data points are presented as mean values and error bars indicate standard deviations obtained from triplicate (*n = 3*) measurements (some error bars are smaller than the data point markers).
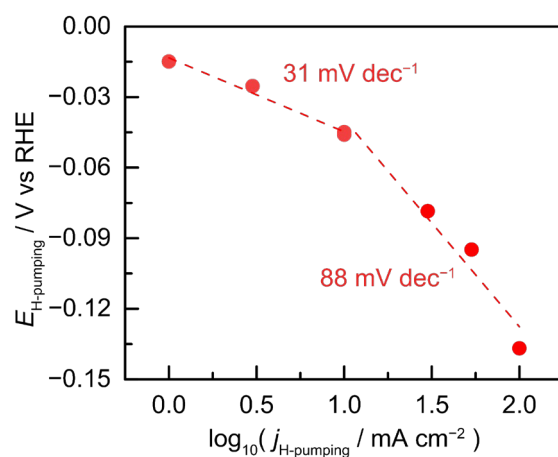
Supplementary Figure 8. Potential-current relationship observed at the H-pumping interface when the analytical interface is held at the open circuit potential. Potentials were measured with a Ag/AgCl reference electrode calibrated to the RHE.
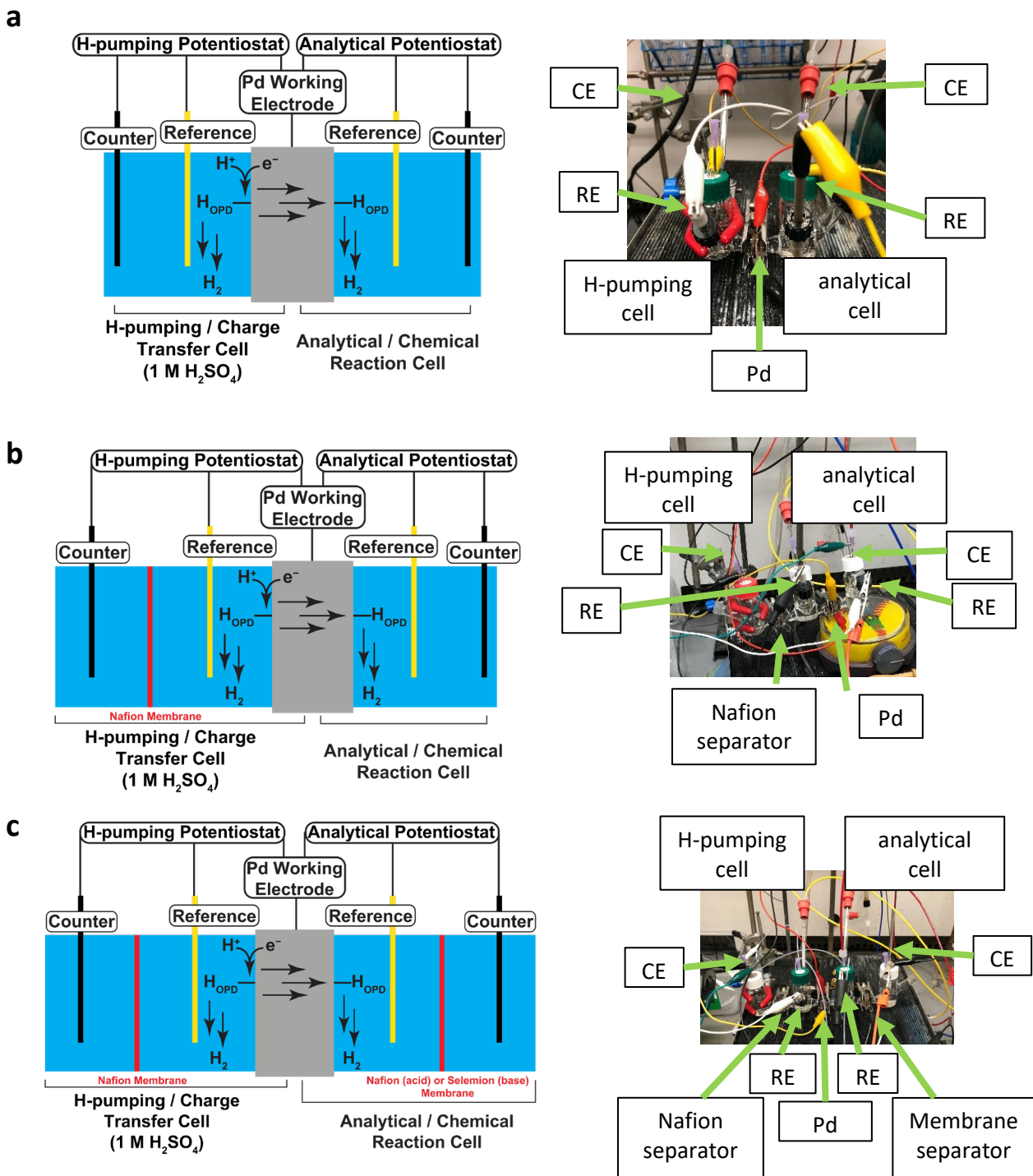
Supplementary Figure 9. Illustrations and photographs of the three different electrochemical double cell configurations **(a)** 2 compartment cell **(b)** 3 compartment cell and **(c)** 4 compartment cell. RE and CE refer to the reference and counter electrodes respectively.

Supplementary References

1. Schreier, M., Yoon, Y., Jackson, M. N. & Surendranath, Y. Competition between H and CO for Active Sites Governs Copper-Mediated Electrosynthesis of Hydrocarbon Fuels. *Angew. Chem.* **130**, 10378–10382 (2018).

2. Schmickler, W. & Santos, E. *Interfacial Electrochemistry*. (Springer Science & Business Media, 2010).